Journal of Power Sources 196 (2011) 1872–1879

Contents lists available at ScienceDirect

Journal of Power Sources

journal homepage: www.elsevier.com/locate/jpowsour

High performance praseodymium nickelate oxide cathode for low temperature solid oxide fuel cell

Claire Ferchaud [a], Jean-Claude Grenier [a], Ye Zhang-Steenwinkel [b], Marc M.A. van Tuel [b], Frans P.F. van Berkel [b], Jean-Marc Bassat [a,*]

[a] Institut de Chimie de la Matière Condensée de Bordeaux (ICMCB-CNRS), Université Bordeaux I, 87 av. du Dr. A. Schweitzer, 33608 Pessac-Cedex, France
[b] Energy Research Centre of the Netherlands (ECN), P.O. Box 1, 1755 ZG Petten, The Netherlands

ARTICLE INFO

Article history:
Received 24 June 2010
Received in revised form 8 September 2010
Accepted 16 September 2010
Available online 22 September 2010

Keywords:
Solid oxide fuel cell (SOFC)
Cathode
Praseodymium nickelate oxide
Impedance spectroscopy
Cell performance test

ABSTRACT

The praseodymium nickelate oxide $Pr_2NiO_{4+\delta}$, a mixed conducting oxide with the K_2NiF_4-type structure, was evaluated as cathode for low temperature solid oxide fuel cells (T = 873 K). The electrochemical performance of the cathode has been improved by optimization of the microstructure of the porous cathode combined with the use of a ceria barrier layer in between the cathode and zirconia electrolyte. Both low polarization and ohmic resistances were obtained using $Pr_2NiO_{4+\delta}$-powders with a median particle size of 0.4 μm, and sintering the screen printed layer at a sintering temperature of about 1353 K for 1 h. These manufacturing conditions resulted in a cathode microstructure with well established connections between the cathode particles and good adhesion of the cathode on the electrolyte. Full-sized anode supported cells have been manufactured using the same process conditions for the $Pr_2NiO_{4+\delta}$ cathode and tested. The best results were obtained when using a dense $Ce_{0.8}Gd_{0.2}O_{1.9}$ (20CGO) barrier layer. While a complete optimization of the cell preparation has not yet been achieved, the electrochemical performances of anode supported cells with $Pr_2NiO_{4+\delta}$ are higher than those with the well known state-of-the-art $La_{0.6}Sr_{0.4}Fe_{0.8}Co_{0.2}O_{3-\delta}$ (LSFC) material.

1. Introduction

Rare-earth nickelates with the K_2NiF_4-type structure, namely $Ln_2NiO_{4+\delta}$ (Ln = La, Nd, Pr) appear to be promising compounds for applications as cathodes for low-temperature solid oxide fuel cells (LT-SOFCs) as well as oxygen-separation membranes. During the last decade several groups have focused their researches on the development of such materials [1–4]. These materials exhibit mixed electronic and ionic conductivity properties, which is highly desirable for improving the oxygen reduction kinetics, the reaction being delocalized over the whole electrode surface [5].

Measurements of the electrical conductivity at high temperatures were first performed by Boehm et al. [6] on sintered dense ceramics and $Pr_2NiO_{4+\delta}$ was found to exhibit the highest value at 873 K (electronic conductivity, σ_e, about 120 S cm^{-1}), which is desirable for application as high performance SOFC cathode.

Large oxygen diffusivity values have been evidenced for $A_2MO_{4+\delta}$-type oxides compared to the perovskite-type. This feature has been assigned to a significant diffusion of the additional oxygen ions mainly occurring in the A_2O_2 layers of the crystal structure of these materials [7,8]. The ionic transport properties of these nickelates was completely characterized through the measurements of the intrinsic bulk oxygen diffusion coefficient (D^*) and of the oxygen exchange coefficient at the surface of the material (k) using O^{16}/O^{18} isotopic exchange [9] or relaxation conductivity. Among the different nickelate compositions $Ln_2NiO_{4+\delta}$ (Ln = La, Nd, Pr), $Pr_2NiO_{4+\delta}$ exhibits the highest D^* value at 873 K (2.5×10^{-8} cm^2 s^{-1}) [6] and a k value around 5×10^{-7} cm^2 s^{-1}, which is about the same order of magnitude as that measured for $Nd_2NiO_{4+\delta}$ and $La_2NiO_{4+\delta}$ [6].

Furthermore, $Pr_2NiO_{4+\delta}$ shows the largest amount of interstitial oxygen, reflected by the δ value ($\delta \sim 0.22$ at room temperature); this value is correlated to the size of the rare-earth cation, Pr^{3+} having the smallest ionic radius inducing large structural stresses that are released by oxygen insertion [10].

Thermo-gravimetric analysis in air revealed a slight decrease of interstitial oxygen ions (δ) for $Pr_2NiO_{4+\delta}$. At increasing temperature, the material is thermally stable up to at least 1273 K [6]. In addition, a structural transition (from orthorhombic to tetragonal symmetry) has been evidenced, at about 723 K [11–13]. This is characterized by both a small oxygen loss and an order–disorder transition for the interstitial oxygen atoms. A split-atom model for the apical oxygen was proposed to simulate their strong anharmonic motion in the $Pr_2O_{2+\delta}$ layers above 723 K and the interstitial oxygen atoms have

* Corresponding author. Tel.: +33 0 540002753; fax: +33 0 540002761.
E-mail address: bassat@icmcb-bordeaux.cnrs.fr (J.-M. Bassat).

0378-7753/$ – see front matter © 2010 Elsevier B.V. All rights reserved.
doi:10.1016/j.jpowsour.2010.09.036

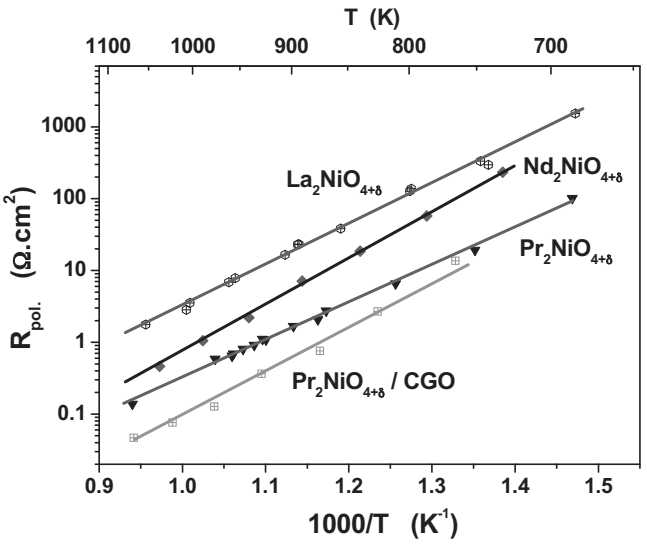

Fig. 1. Arrhenius plots of R_{pol} for $Ln_2NiO_{4+\delta}$ (Ln = La, Nd and Pr) cathodes in symmetrical cells.

been found to be distributed between two sites. More recently, this has been confirmed by modelling the diffusion path of oxide ions that showed the anisotropic thermal motions of the oxygen atom in this layer, which explains the high oxygen permeability of this oxide [14].

Under oxygen atmosphere, $Pr_2NiO_{4+\delta}$ undergoes an oxidation process at about 1073 K resulting in a reversible decomposition into $Pr_4Ni_3O_9$ and $PrO_{1.71}$ [15,16]; this has been also correlated to a somewhat easy mobility of the apical oxygen atoms in the structure [17]. However, it does not appear to be penalizing for the SOFC application, because under cathodic polarization, the local oxygen pressure is lower than atmospheric pressure [18].

Therefore, in general, on basis of these specific features, $Pr_2NiO_{4+\delta}$ has gained a large interest as cathode material for SOFC during the last few years. This is illustrated in Fig. 1; the polarization resistances R_{pol} of the $Ln_2NiO_{4+\delta}$ (Ln = La, Nd and Pr) compounds obtained from impedance spectroscopy measurements on symmetrical cells show that the smallest values are obtained for the Pr phase.

Recently, two comparative sets of data on Nd and La nickelates have also been published by Lalanne et al. [19] and by Laberty et al. [20], respectively. Both studies were achieved for complete cells at 1073 K. The first one, concerning a cell consisting of Ni/8YSZ cermet, 8YSZ as electrolyte, neodymium nickelate $Nd_2NiO_{4+\delta}$ as cathode and $La_{0.6}Sr_{0.4}CoO_{3-\delta}$ (LSC) as the current collector, evidenced a degradation of the performances with time caused by a delamination of the cathode. This problem was avoided when using a ceria based interface between the nickelate and the electrolyte. The second study of Laberty et al. showed a large improvement of the maximum power when using a lanthanum nickelate/Sm-doped ceria (SDC) composite instead of pure nickelate. Such recent results on nickelates agree with previous reports concerned with other cathode materials, *i.e.* an interface of doped ceria is generally used in the preparation of the SOFCs in order to diminish the thermal expansion mismatch but mainly to prevent the reactivity between the zirconia electrolyte and the cathode. This has been especially claimed for the LSFC-cathode [21–25]. With respect to the nickelates, we evidenced that the poor electrochemical performance of $La_2NiO_{4+\delta}$ that has been directly screen-printed on YSZ electrolyte, is due to the formation of the insulating pyrochlore-type oxide [26]. The addition of a ceria layer is beneficial as shown in Fig. 1, the polarization resistance of the praseodymium nickelate cathode being lowered by the addition of a ceria interface layer.

The aim of this paper is to report the improvement in electrochemical performances of $Pr_2NiO_{4+\delta}$ cathodes at an operating temperature of 873 K by designing an optimized microstructure, which has been achieved by variation of three preparation parameters: (1) the ink composition; (2) the particle size of the starting material; (3) the sintering temperature of the screen printed cathode. Also, the influence of two different ceria interface layers has been investigated. Finally, the cell performance of the full-sized anode supported cells using $Pr_2NiO_{4+\delta}$ as cathode has been tested and their performances are compared to the-state-of-the-art cell consisting of LSFC as cathode.

2. Experimental

2.1. Synthesis and characterizations of $Pr_2NiO_{4+\delta}$ oxides and ceria barrier layers: powders and inks

Commercial submicronic $Pr_2NiO_{4+\delta}$ oxide powders were synthesized by Marion Technologies Company using the auto-ignition route [27]. The powders as received were ball milled in order to obtain different median particle sizes, the aim being to study the influence of this parameter on the microstructure of the final electrode. Three sizes were selected, *i.e.* 0.2, 0.4 and 0.7 μm. Dilatometry measurements were performed on pressed pellets made of powders with sizes 0.4 and 0.7 μm, using a dilatometer (Netzsch DIL402C), with the aim to determine the onset of sintering. Experiments were performed under air, with a heating rate of 100 K h^{-1}, up to 1573 K.

Ceria powders, $Ce_{0.8}Gd_{0.2}O_{1.9}$ (CGO, Rhodia) and $Ce_{0.8}Y_{0.2}O_{2-\delta}$ (YDC, Praxair) have been used for the ceria barrier layer development. Screen print pastes have been prepared by mixing the ceria powders into a dispersant aid and binder system using a Dispermat milling system. The screen print paste formulations have been optimized for high green density ceria layers in order to diminish the shrinkage during sintering which results in less cracking on the layer and higher sintered densities. Optionally, a sintering aid in the form of a cobalt nitrate salt was added to the screen printing pastes, aiming for high density ceria layers at lower sintering temperature. The Co-concentration is approximately 0.6 mol% of the total amount of ceria in the screen print paste [28].

For the cathodes, three screen-print inks were prepared; one in CNRS using the 0.4 μm powder with a mass percentage of 70% added in a terpineol medium, two other ones at ECN using a home made binder and the 0.2 and 0.7 μm powders, respectively, with a mass percentage of about 40%.

2.2. Symmetrical cell tests

2.2.1. Symmetrical cell fabrication

The symmetrical cells were made starting from 3% yttria doped zirconia (TZ3Y) electrolyte produced by ECN via a tape casting process, leading to sintered electrolyte layers with a thickness of 90–100 μm and a diameter of 25 mm. YDC interface layers were screen-printed on both sides of the electrolyte, and sintered at 1673 K for 1 h in air with a controlled heating rate of 100 K h^{-1}, resulting in ceria layer thicknesses of approximately 2–4 μm. Subsequently, $Pr_2NiO_{4+\delta}$ ink was screen-printed on top of the YDC interlayer and sintered at various temperatures, with heating rate of 100 K h^{-1}, in the temperature range of 1303–1503 K, for 1 h. The aim is to study the influence of the sintering temperature on the performance of the cathode materials. The resulted cathode layer thickness is about 25–30 μm.

2.2.2. Microstructural characterizations

A scotch tape test using a Magic 3M-type (19 mm wide) was systematically performed to determine the adherence of the cathode.

When the adherence of the electrode was not sufficient, the cell was rejected. Such a procedure is in agreement with the standard one as described in the literature [29].

After sintering, the microstructure, surface and cross section of the symmetrical cells were observed by field emission Scanning Electron Microscopy (SEM) using a JEOL JSM 6330F equipped with an EDS detector of Thermo Noran. The porosity values after sintering were determined by two methods:

(i) The inter-granular porosity was calculated from image analysis (using Image J software) of SEM photographs of the electrode.
(ii) The total porosity was deduced from the density of the electrode determined from geometric, measured weight and theoretical density.

The difference between total density and inter-granular values was assumed to be due to cracks or more generally to textural imperfections ("T.I." in the following) in the electrode.

2.2.3. Electrical and electrochemical characterizations

First, electrical conductivity measurements were performed at room temperature using the four probes technique in order to determine the lateral resistance of the electrodes. Lower value of resistance indicates better microstructure of cathode with respect to improved particle-to-particle electrical connectivity.

Electrochemical measurements on the symmetrical cells were carried out by impedance spectroscopy. Impedance diagrams were recorded from 1073 K down to 873 K, every 50 K, using a Solartron 1260 frequency response analyzer (the applied frequencies were in the range of 0.01 Hz to 1 MHz with signal amplitude of 10 mV). Au grids (1024 mesh) were used as current collectors. The impedance measurements were performed under OCV conditions with synthetic 100 ml min^{-1} air (20% O_2 and 80%N_2). Curve fittings were performed using the Zview software.

The impedance diagrams could be decomposed, in the frequency range, into two main contributions: the first one being the intercept of the response with the real axis at high frequency (HF), corresponds to the ohmic part (R_{ohm}) of the cell, the second one being the sum of two arcs, the MF and LF contributions, corresponds to the polarization resistance (R_{pol}) of the electrode. Both normalized resistance values were calculated with respect to the surface of the symmetrical cells (active surface area = 3.8 cm^2).

2.3. Cathode integration in anode supported SOFC

In parallel, full-sized anode supported cells were manufactured with $Pr_2NiO_{4+\delta}$ as cathode and tested on their cell performance. The obtained results were compared to the standard cells involving the-state-of-the-art LSFC as cathode materials.

2.3.1. Cell fabrication

The $Pr_2NiO_{4+\delta}$ cathodes in combination with the ceria barrier layer were screen-printed on the squared-shaped 5 cm × 5 cm anode-supported half cells. These half cells consisted of a Ni/8YSZ anode-substrate (approximately 550 μm), a Ni/8YSZ anode functional layer of 5–10 μm and a 3–5 μm thick 8YSZ electrolyte layer. A CGO or YDC layer was screen-printed on the half cells. Subsequently, it has been sintered for 1 h at 1573 K and 1673 K, respectively. Two different CGO inks were used: the first one was a standard composition while the second one contained additional cobalt oxide which is known as sintering aid for CGO from previous reports of Kleinlogel and Gauckler [30] and Mai et al. [31]. The $Pr_2NiO_{4+\delta}$ (powder with a median particle size of 0.4 μm) pastes were screen-printed on the anode supported half cells, followed by sintering at 1373 K for 1 h. That resulted in a layer thickness of ca. 30 μm with active cell area about 10 cm^2. The performances of the mentioned cells were compared with the-state-of-the-art cell using LSFC (Rhodia) as cathode materials. This LSFC have been sintered at 1373 K for 1 h, resulting in a layer thickness of ca. 30–40 μm.

The compositions of the five single cells used in this study are as follows:

$Pr_2NiO_{4+\delta}$	ASC//CGO (thick, 2.3 μm)//$Pr_2NiO_{4+\delta}$
	ASC//CGO (thin, 1.3 μm)//$Pr_2NiO_{4+\delta}$
	ASC//YDC (1.3 μm)//$Pr_2NiO_{4+\delta}$
$L_{0.6}Sr_{0.4}Fe_{0.8}Co_{0.2}O_{3-\delta}$	ASC//CGO(Co-ink)//LSFC

The post test analysis has been performed by SEM on cross sections using a JEOL HSM-6330F field emissions type Scanning Electron Microscope.

2.3.2. Impedance measurement on single cells

The cell performance was evaluated in a 5 cm × 5 cm cell housing with corrugated ceramic channels for good gas distribution. Platinum (Pt) meshes were used for current collection on both anode and cathode sides. A weight of 2.5 kg was placed on top of the cell housing in order to obtain better contact between the current collector and the electrodes. The cell anodes were reduced after heating in 5% H_2 diluted in N_2, at 1073 K. The anode side was flushed with room temperature humidified hydrogen with a flow rate of 500 ml min^{-1}. On the cathode side, synthetic flowing air (20% O_2 and 80% N_2) was supplied as oxidant with flow rates of 400 ml min^{-1} and 1600 ml min^{-1}, respectively. The current density and voltage values were recorded as a function of operating temperatures, from 1073 K down to 873 K. The impedance measurements were performed for all tested cells at a current density of 0.4 A cm^{-2}, using a Solartron Schlumberger frequency response analyzer (FRA) model 1255 coupled with a Schlumberger Potentiostat model 1287A. The applied frequencies were in the range of 0.01 Hz to 1 MHz with signal amplitude of 10 mV. The obtained Nyquist plots were fitted using the Zview2 fitting program. The contributions of the ohmic and electrode resistances to the total cell losses were determined from these data.

3. Results and performances

3.1. Symmetrical cell tests

The symmetrical cells consisted of a 20YDC layer between YSZ and the nickelate cathode. The optimization of the cathode microstructure was performed on such cell configuration by variation of particle size, ink composition and sintering temperatures. The following paragraphs describe the effects of those parameters on cathode microstructure and electrochemical performance.

3.1.1. Influence of particle size distribution and sintering temperatures

It is well known that for LSFC-type cathodes the best electrochemical performances are obtained using small and spherical particles, with a narrow size distribution [32]. For this reason, first experiments were carried out using inks made with the nickelate powder having a particle size of 0.2 μm, the sintering temperature ranging in between 1503 K and 1703 K. However, such experiments were unsuccessful: whatever the sintering temperature, cracks were observed on the surface of the samples, their size increasing with temperature, from about 1 mm till the complete removing of the layer at the highest temperatures. Using this powder with such small particle size results in a large shrinkage of the cathode layer leading to a detrimental mismatch between the YDC and cathode layers. Correspondingly the textural imperfections number ("T.I." percentage) calculated as described in paragraph 2.2.2, was very high, from 14% to 36%. Such defects were not observed on green samples. Moreover, the cathode layer can be removed easily

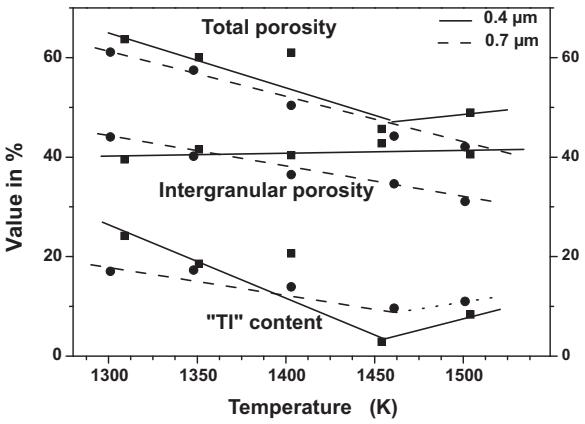

Fig. 2. Total porosity, inter-granular porosity and "T.I." content measured for cathode materials on a symmetrical cell configuration, as a function of the sintering temperatures for cathode materials with two particle sizes: 0.4 and 0.7 µm, respectively.

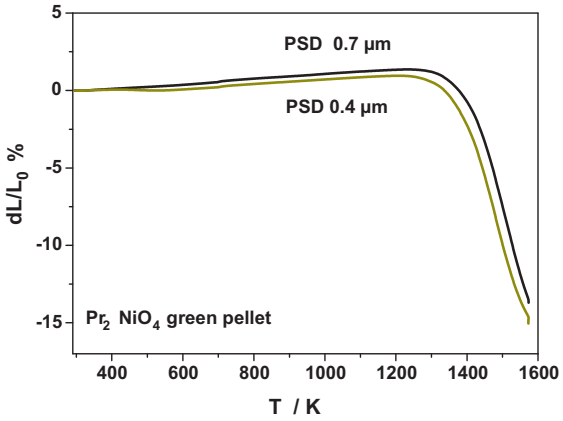

Fig. 4. Dilatometry measurements for $Pr_2NiO_{4+\delta}$ powders with sizes 0.4 and 0.7 µm.

from the surface of the electrolyte by the scotch tape test; consequently no electrochemical measurement could be performed on such symmetrical cells.

Then, sintering experiments were performed on samples made using powders with average particle sizes of 0.4 and 0.7 µm, respectively, at a temperature range of 1703–1503 K. In Fig. 2, correlation between total and inter-granular porosities and the resulting "T.I." content is shown. For both powders, the lowest "T.I." content is obtained at a sintering temperature around 1453 K, being about 3% and 9% for the powders with average particles size of 0.4 and 0.7 µm, respectively.

SEM images of sintered electrodes for both powders are shown in Fig. 3a and b. The inter-granular microstructure analysis of the cathodes evidences a progressive densification of the layer at increasing sintering temperature up to 1503 K. The formation of neck growth at sintering temperatures above 1353 K is in agreement with the dilatometry measurements (Fig. 4). The onset sintering temperatures are respectively 1378 K for the 0.4 µm $Pr_2NiO_{4+\delta}$ powder and 1408 K for the 0.7 µm one. It slightly increases with the particle size distribution of the powder. This indicates that for optimum lateral conductivity in the cathode, the sintering temperature should be higher than 1408 K. This has been demonstrated by the lateral conductivity measurements at room temperature for the cathodes sintered at varying temperatures. The lateral conductivity increased with increasing sintering temperatures.

3.1.2. Impedance measurements

Typical Nyquist plots obtained at $T = 873$ K for $Pr_2NiO_{4+\delta}$ with average particle size of 0.4 µm are shown in Fig. 5. All data

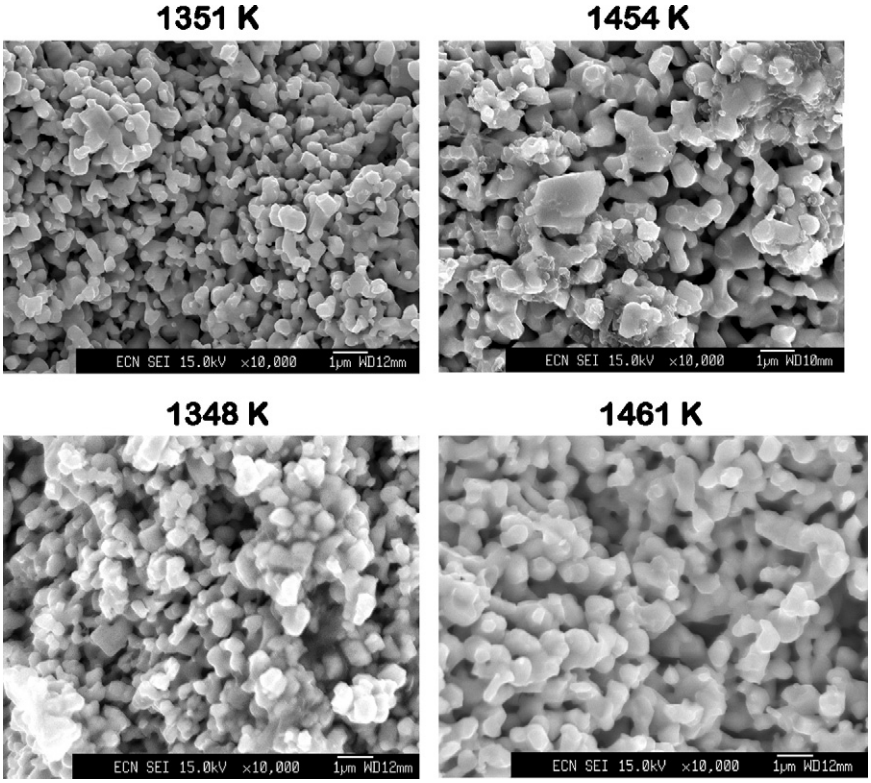

Fig. 3. (a) Change in the cathode microstructure as function of sintering temperatures for $Pr_2NiO_{4+\delta}$ powders with median particle size 0.4 µm; (b) change in the cathode microstructure as function of sintering temperatures for $Pr_2NiO_{4+\delta}$ powders with median particle size 0.7 µm.

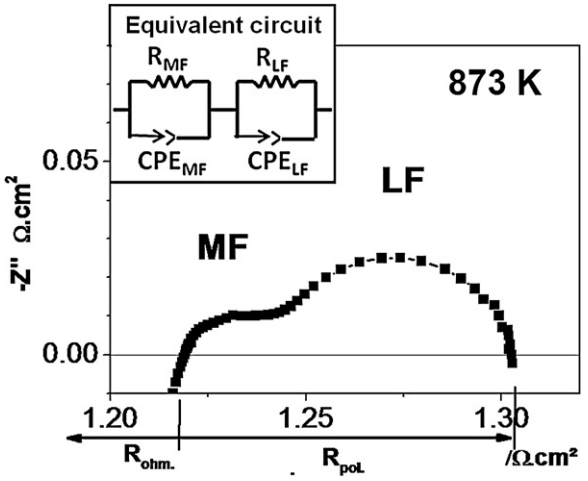

Fig. 5. Typical impedance spectrum (T = 873 K) of a symmetrical cell with 20YDC interface layer and $Pr_2NiO_{4+\delta}$ cathode (particle size 0.4 μm) sintered at 1453 K. Ohmic (R_{ohm}) and electrode polarization (R_{pol}) resistances are given in (cm^2. The corresponding equivalent circuit used for fitting R_{pol} is shown in the inset.

at medium and low frequencies corresponding to the electrode contribution were fitted on the basis of an equivalent circuit constituted of two resistance – constant phase elements (R – CPE) in parallel, associated in series. Referring to previous works [33], they can be interpreted as follows: (i) the first semi-circle in the middle frequency regime (MF) is assigned to the transfer of O^{2-} ions from the electrode to the electrolyte on the basis of its small capacitance and (ii) the large depressed arc at low frequency (LF impedance) characterizes the oxygen adsorption/dissociation steps overlapped with diffusion processes.

The ohmic and polarization resistances of the investigated $Pr_2NiO_{4+\delta}$ with average particle size of 0.4 μm as measured at 873 K are plotted in Fig. 6a, as a function of the sintering temperatures. Both the obtained R_{ohm} and R_{pol} values decrease with increasing sintering temperatures. The lowest resistance values can be observed at a sintering temperature of 1454 K. Similar behaviour of the resistance values as function of sintering temperature has been obtained for the cathode material with average particle size of 0.7 μm. The dependency of the ohmic resistance value on the sintering temperature can be explained by the formation of better established particle-to-particle connectivity or better neck growth between the cathode particles with increasing sintering temperature as also observed in SEM-pictures of the cathode microstructures (see Fig. 3b). Improved neck growth between the cathode particles results in better electronic lateral conductivity of the cathode layer, which consequently results in lower contribution of the cathode lateral resistance to the total ohmic losses. Fig. 6b confirms that the lateral resistance value, as measured by a four point method at room temperature, decreases with increasing sintering temperature, resulting in the lowest lateral resistance values at a sintering temperature equal or higher than 1453 K. Assuming that the observed trend between lateral resistance and sintering temperature can be translated from room temperature to the actual operating temperature of 873 K value, it is clear from Fig. 6a and b that both the lateral resistance and ohmic resistance follow largely the same trend as a function of sintering temperature. This indicates that the neck growth between the cathode particles is crucial for obtaining a well-performing cathode.

A further indication of the importance of cathode microstructure and lateral resistance on the ohmic losses can be observed in Fig. 7. This figure shows an Arrhenius plot of the ohmic resistance of the different cathode samples as a function of operating temperature. For comparison this figure also includes the ohmic losses (R_{ohm})

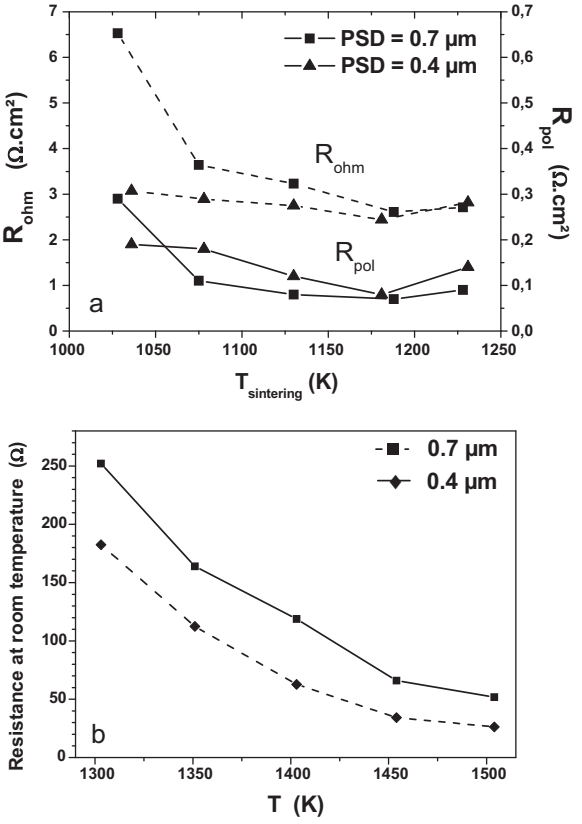

Fig. 6. Ohmic and polarization resistances measured on a symmetrical cell using $Pr_2NiO_{4+\delta}$ (0.4 μm) at 873 K: (a) the ohmic and polarization resistance as function of the sintering temperatures; (b) the surface resistance of the cathode at room temperature as function of the sintering temperatures.

measured for the tetragonal zirconia TZ3Y electrolyte (platinum electrodes were deposited on each side and sintered at T = 1173 K), which is being used in the measured symmetrical cells. This figure demonstrates that the ohmic resistance of the cathode with sintering temperature higher than 1450 K, *i.e.* the cathodes with lowest lateral resistance, follows the same Arrhenius behaviour as the resistance of the TZ3Y-electrolyte, while the samples with lower sintering temperature, *i.e.* the cathodes with higher lateral resis-

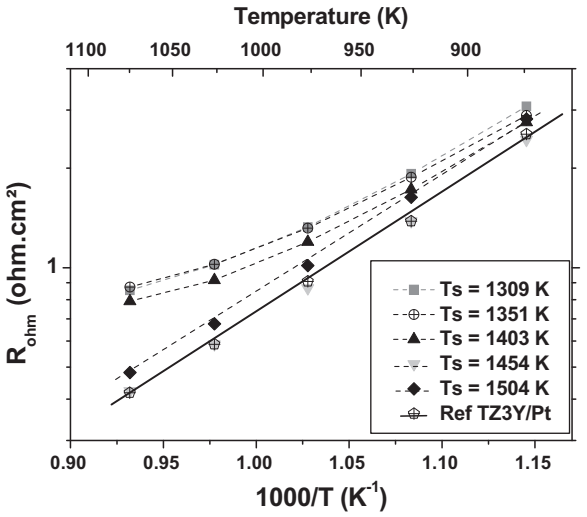

Fig. 7. R_{ohm} as function of operating temperatures for the $Pr_2NiO_{4+\delta}$ cathode with size 0.4 μm sintered at various temperatures. Values measured for the electrolyte TZ3Ywith Pt electrodes (sintered at 1173 K) are included for comparison.

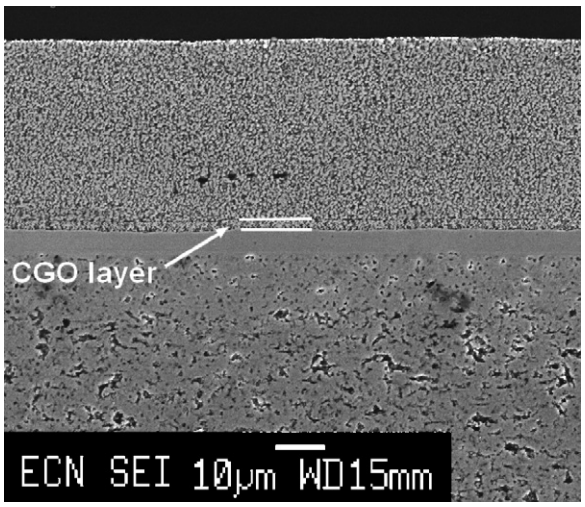

Fig. 8. SEM image (cross section) of a single cell ASC//CGO (ink with Co addition)//$Pr_2NiO_{4+\delta}$ (0.4 µm).

tance values, do not follow Arrhenius behaviour but show severe bending of the resistance curves at high operating temperatures. It is noteworthy that the symmetrical cell involving $Pr_2NiO_{4+\delta}$ cathode sintered at 1454 K and 1504 K, *i.e.* the cathodes with the lowest lateral resistance value, shows similar R_{ohm} value as expected for the TZ3Y-electrolyte, being 2.5 Ω cm^2 at 873 K, suggesting that no detectable contributions to R_{ohm} originate from cathode lateral resistance or both TZ3Y/YDC and YDC/cathode interfaces. The bending of the ohmic resistance for the cathodes with lower sintering temperature indicates that an additional resistance value with less temperature dependency than the TZ3Y electrolyte resistance contributes to the overall ohmic losses. This less temperature dependent additional resistance value might be assigned to the contribution of the lateral resistance of the cathodes to the ohmic losses, as stated before in this chapter.

The behaviour of the polarization resistance as function of sintering temperature follows the same trend as the ohmic resistance (see Fig. 6a). This phenomenon might be explained by the fact that the observed poor lateral resistance values at low sintering temperature will very likely result in poor current density distribution over the cathode–electrolyte interface resulting in inefficient use of electro-catalytically active sites along the cathode–electrolyte interface resulting in higher polarization resistance values.

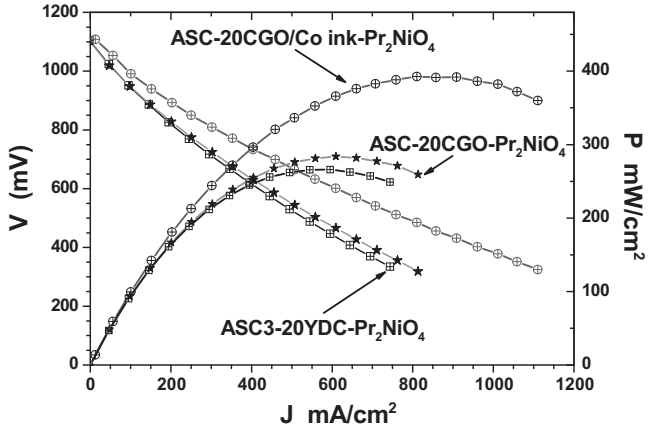

Fig. 9. J-V characteristics and power density of three tested single cells with $Pr_2NiO_{4+\delta}$ (PRN) as cathode. Test conditions: operating temperature is 873 K; gas composition on the anode side: room temperature humidified H_2 (500 ml min^{-1}); cathode side: synthetic air with 400 ml min^{-1} O_2 and 1600 ml min^{-1} N_2.

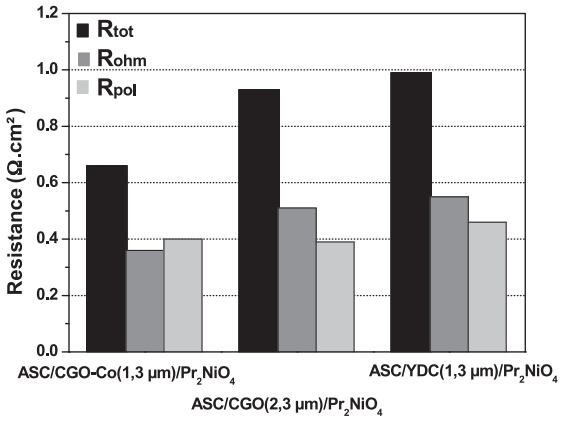

Fig. 10. Total area specific resistance (R_{tot}), ohmic losses (R_{ohm}) and electrode polarization losses (R_{pol}) are given for each cell configuration and has been determined by impedance measurement at 0.4 A cm^{-2} at 873 K.

At cathode sintering temperature higher than 1450 K, both ohmic and polarization resistance values increase as shown in Fig. 6a. Two causes might explain this behaviour. First, high sintering temperature results in a further growth in particles size that lower the active surface to volume ratio, leading to less triple phase boundary points. As a consequence, reduction of catalytically active site for the oxygen reduction reaction may occur. Second, at such sintering temperatures, some reactivity between the cathode and the barrier layer might occur, resulting in formation of a solid state reaction zone with lower oxygen ionic conductivity. After sintering at high temperature a reddish coloured phase between the cathode and the electrolyte has been observed, indicating that an additional reaction zone has been formed. The combination of these two possible explanations result in both decreased oxygen charge transfer and oxygen ionic conductivity over the ceria barrier layer resulting in respectively higher polarization and ohmic resistances.

To conclude, the electrochemical performance of the cathodes can be improved by optimizing the cathode processing parameters, being ink composition, particle size and the sintering temperature. The most promising $Pr_2NiO_{4+\delta}$ cathode has been obtained for the one with average particle size of 0.4 mm and sintered at 1454 K, showing ohmic losses, which can be assigned completely to the TZ3Y-electrolyte, and optimum polarization resistance value of 0.08 Ω cm^2 at an operating temperature

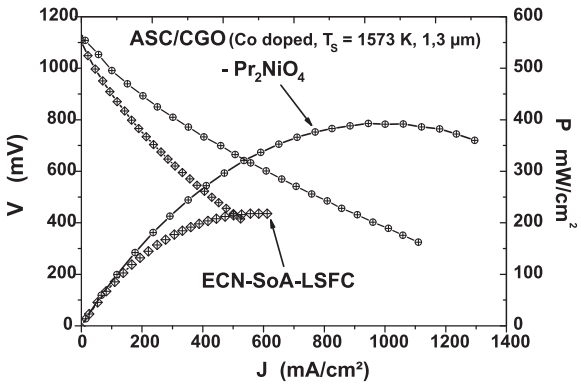

Fig. 11. Cell voltage and power density as function of current density at 873 K with humidified H_2 (500 ml min^{-1}) supplied to anode and synthetic air (400 ml min^{-1} O_2 and 1600 ml min^{-1} N_2) supplied to cathode; ● SoA-LSCF; ▲ ASC-CGO (Co-doped, 1.3 µm)-PRN ($Pr_2NiO_{4+\delta}$); the LSCF and PRN cathodes have been sintered at 1373 K and 1403 K, respectively, for 1 h.

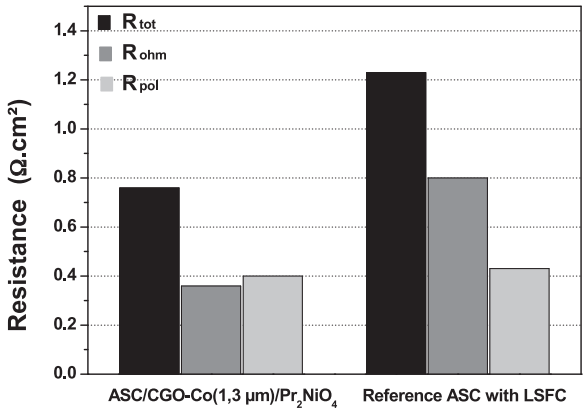

Fig. 12. Ohmic losses (R_{ohm}) and electrode polarization losses (R_{pol}) are given for each cell configuration and has been determined by impedance measurement at 0.4 A cm^{-2} at 873 K.

of 873 K. The resulted polarization resistance is comparable to reported polarization resistance of LSC-cathode materials, which is well-known cathode material for low temperature SOFC [34–36].

3.2. Cell tests

The cell performance of full-sized anode supported cell with praseodymium nickelate as cathode in combination with ceria barrier layer has been investigated. The cell compositions are described in the experimental part. Three types of single cells were studied: (1) with YDC barrier layer (ca. 1.3 μm); (2) with CGO barrier layer without additional sintering aid (ca. 2.3 μm); (3) with CGO barrier layer with sintering aid (ca. 1.3 μm).

SEM image of the cross section of a single cell is shown in Fig. 8. It evidences a good quality of the interfaces on one hand, between YSZ and the doped ceria layer and, on the other hand, between the ceria layer and the porous electrodes.

Fig. 9 shows the J-V characteristics of these three cells at 873 K. Comparable cell performances have been observed for the cells with YDC barrier layer and CGO barrier layer without sintering aid, resulting in a maximum power output density less than 300 mW cm^{-2}. The use of a relatively thin Co-doped CGO barrier layer (1.3 μm) resulted in improved cell performance with a maximum powder output density of ca. 400 mW cm^{-2}. The impedance measurement data shown in Fig. 10 indicates that the main improvement is due to the diminished ohmic resistance by the implementation of the thin CGO layers. The ohmic resistance has been reduced by 30%. Also, the additional sintering aid may result in the better densification of this CGO barrier layer that additional contributes to lower ohmic resistance values [28]. The use of YDC resulted in higher ohmic resistance compared to CGO. That is due to its lower ionic conductivity compared to CGO at 873 K [37].

For comparison, the reference cell with LSFC as cathode has been included in Fig. 11. This figure shows that a peak power density of ca. 400 mW cm^{-2} has been obtained for the cell with the optimized $Pr_2NiO_{4+\delta}$ cathode combined with the thin CGO barrier layer, while 184 mW cm^{-2} was measured for the reference cell. Significantly improved cell performance has been obtained by the simultaneous implementation of a CGO barrier layer and praseodymium nickelate cathode. The main improvement as shown in Fig. 12 is due to the reduction of both R_{ohm} and R_{pol}, in particular, the R_{ohm}. These performances can be further improved when sintering the cathode according to the optimized process described in part 2, which is still in progress.

4. Conclusion

In this work, the optimization of the microstructure of praseodymium nickelate, $Pr_2NiO_{4+\delta}$ (PRN), aiming for high and stable performance, has been carried out on a symmetrical cell configuration with YDC as interface barrier layer. Three steps with respect to the optimization of the microstructure have been executed: (1) optimized the particle size distribution; (2) improved cathode paste composition and (3) optimized the sintering temperature. The optimum sintering temperature results in diminished polarization and ohmic part that can be explained by the formation of the neck growth in the cathode layer, leading to a good electrical connectivity that results in efficient use of the electrochemical active cathode barrier layer interface. With the optimization developed here, both adhesion of the cathode on the electrolyte and improvement of the cathode microstructure were simultaneously achieved. However, it should be mentioned that at higher sintering temperature solid state reaction between cathode and interface layer might occur, resulting in formation of a reaction zone with lower oxygen ionic conductivity. The $Pr_2NiO_{4+\delta}$ powder with average particle size of 0.4 μm and sintered at 1403 K has been determined to be the most performing cathode material for SOFC operating at 873 K. A polarization resistance value of 0.08 Ω cm^2 along with an ohmic resistance value of 2.5 Ω cm^2 has been obtained on a symmetrical cell configuration at 873 K. The observed ohmic resistance is similar to the expected value of TZ3Y electrolyte at 873 K, suggesting that the ohmic contribution of the interfaces (TZ3Y/YDC and YDC/cathode) is negligible compared to the ohmic resistance of TZ3Y electrolyte at the mentioned operating temperature.

The choice of the applied ceria barrier layer is of importance for the single anode supported cell performance at lower operating temperature. CGO layer shows to be a better barrier layer compared to YDC, since its ionic conductivity is higher at an operating temperature of 873 K. Further, the addition of sintering aid and reduced barrier layer thickness of CGO layer result in significantly improved cell performance. The main improvement is due to the further diminished ohmic contributions. The best cell performance has been obtained for the cell combined with a thin screen-printed Co-doped GCO layer with a maximum power output density of ca. 400 mW cm^{-2} at 873 K.

Acknowledgment

Financial support from the EC within the integrated project SOFC600 (Contract No. 020089) is gratefully acknowledged.

References

[1] E. Boehm, J.M. Bassat, M.C. Steil, P. Dordor, F. Mauvy, J.C. Grenier, Solid State Sci. 5 (2003) 973.
[2] J.A. Kilner, C.K.M. Shaw, Solid State Ionics 154–155 (2002) 523.
[3] V.V. Vashook, I.I. Yushkevich, L.V. Kokhanovsky, L.V. Makhnach, S.P. Tolochko, I.F. Kononyuk, H. Ullmann, H. Altenburg, Solid State Ionics 119 (1999) 23.
[4] D.C. Zhu, X.Y. Xu, S.J. Feng, W. Liu, C.S. Chen, Catal. Today 82 (2003) 151.
[5] M. Kleitz, F. Petitbon, Solid State Ionics 92 (1996) 65.
[6] E. Boehm, J.M. Bassat, P. Dordor, F. Mauvy, J.C. Grenier, P. Stevens, Solid State Ionics 176 (2005) 2717.
[7] S.J. Skinner, J.A. Kilner, Solid State Ionics 135 (2000) 709.
[8] J.M. Bassat, P. Odier, A. Villesuzanne, C. Marin, M. Pouchard, Solid State Ionics 167 (2004) 341.
[9] J.M. Bassat, M. Petitjean, J. Fouletier, C. Lalanne, G. Caboche, F. Mauvy, J.C. Grenier, Appl. Catal. A: Gen. 289 (2005) 84–89.
[10] D.J. Buttrey, P. Ganguly, J.M. Honig, C.N.R. Rao, R.R. Schartman, G.N. Subanna, J. Solid State Chem. 74 (1988) 233.
[11] M.T. Fernandez-Diaz, J.L. Martinez, J. Rodriguez-Carvajal, Solid State Ionics 63–65 (1993) 902.
[12] C. Allançon, A. Gonthier-Vassal, J.M. Bassat, J.P. Loup, P. Odier, Solid State Ionics 74 (1994) 239.
[13] C. Allançon, J. Rodriguez-Carvajal, M.T. Fernandez-Diaz, P. Odier, J.M. Bassat, J.P. Loup, J.L. Martinez, Z. Phys. B 100 (1996) 85–90.

[14] M. Yashima, M. Enoki, T. Wakita, R. Ali, Y. Matsushita, F. Izumi, T. Ishihara, J. Am. Chem. Soc. 130 (2008) 2762–2763.
[15] P. Odier, C. Allançon, J.M. Bassat, J. Solid State Chem. 153 (2000) 381.
[16] A.V. Kovalevsky, V.V. Kharton, A.A. Yaremchenko, Y.V. Pivak, E.N. Naumovich, J.R. Frade, J. Eur. Ceram. Soc. 27 (2007) 4269–4272.
[17] J. Choisnet, J. Solid State Chem. 147 (1999) 379.
[18] J.C. Grenier, F. Mauvy, C. Lalanne, J.M. Bassat, F. Chauveau, J. Mougin, J. Dailly, M. Marrony, ECS Trans. 25 (2) (2009) 2537–2546.
[19] C. Lalanne, G. Prosperi, J.M. Bassat, F. Mauvy, S. Fourcade, P. Stevens, M. Zahid, S. Diethelm, J. Van Herle, J.C. Grenier, J. Power Sources 185 (2008) 1218–1224.
[20] C. Laberty, et al., Electrochem. Solid State Lett. 10 (2007) B170.
[21] C.C. Chen, M.M. Nasrallah, H.U. Anderson, in: S.C. Shingal, H. Iwahara (Eds.), PV93-4, The Electrochemical Society Proceeding Series, Pennington, NJ, p. 598.
[22] H.Y. Tu, Z. Takeda, N. Imanislli, O. Yamamoto, Solid State Ionics 117 (1999) 277.
[23] Hiroyuki, et al., Electrochem. Solid State Lett. 2 (9) (1999) 428–430.
[24] L. Qui, et al., Solid State Ionics 158 (2003) 55–65.
[25] Uhenbruck, et al., Thin Solid Films 515 (2007) 4053–4060.
[26] A. Aguadero, J.A. Alonso, M.J. Escudero, L. Daza, Solid State Ionics 179 (2008) 393–400.
[27] http://www.mariontechnologies.com/nanomateriaux/index.php.
[28] F.P.F. Van Berkel, Y. Zhang-Steenwinkel, G.P.J. Schoemakers, M.M.A. Van Tuel, G. Rietveld, ECS Trans. 25 (2) (2009) 2717.
[29] G.C. Schwartz et, K.V. Srikrishnan, Handbook of Semi-conductor Interconnection Technology, second edition, Taylor and Francis Group, CRC Press, 2006, p. 89.
[30] C. Kleinlogel, L.J. Gauckler, Solid State Ionics 135 (2000) 567.
[31] A. Mai, et al., Solid State Ionics 177 (2006) 2103.
[32] K. Murata, T. Fukui, H. Abe, M. Naito, K. Nogi, J. Power Sources 145 (2005) 257–261.
[33] F. Mauvy, C. Lalanne, J.M. Bassat, J.C. Grenier, H. Zhao, L. Huo, P. Stevens, J. Electrochem. Soc. 153 (2006) A1547–A1553.
[34] C. Peters, A. Weber, E. Ivers-Tiffée, J. Electrochem. Soc. 155 (7) (2008) B730.
[35] E. Ivers-Tiffée, U. Guntow, J. Hayd, B. Rüger, A0403, 8th European Solid Oxide Fuel Cell Forum, Lucerne, Switzerland, 2008.
[36] F. van Berkel, S. Brussel, M. van Tuel, G. Schoemakers, B. Rietveld and P.V. Aravind, 8th European Solid Oxide Fuel Cell Forum, Lucerne, Switzerland, 2008.
[37] V.V. Kharton, F.M. Figueiredo, L. Navarro, E.N. Naumovich, A.V. Kovalevsky, A.A. Yaramchenko, A.P. Viskup, A. Carneiro, F.M.B. Marques, J.R. Frade, J. Mater. Sci. 36 (2001) 1105.